JOURNAL OF GUIDANCE, CONTROL, AND DYNAMICS
Vol. 29, No. 4, July–August 2006

# Path-Oriented Control/Display Augmentation for Perspective Flight-Path Displays

C. Borst,* M. Mulder,† M. M. van Paassen,‡ and J. A. Mulder§
*Delft University of Technology, Delft, The Netherlands*

**Flight-path predictor display augmentation and flight-path vector control augmentation concepts have been developed to improve pilot performance and reduce workload with a perspective flight-path display. A recent comparison study conducted at the Delft University of Technology showed a preference for control augmentation, although some improvements could still be made. Pilots command the direction of the aircraft motion and, because in curved trajectories the direction must constantly change, they are required to hold the stick deflected during turns. It is also not clear how much stick deflection is needed during a particular turn. This paper discusses an augmentation concept that addresses these issues. A path-oriented control and display augmentation is described in which the pilot commands the curvature of the aircraft future trajectory, shown as a perspective wireframe on the display. Results of an experiment, conducted in a fixed-base simulator, indicate that although pilot performance improved with this path-augmentation concept, pilot workload and control activity increased. A surprising result of the path-augmentation concept was the relatively large improvement in vertical pilot performance; its primary goal was to improve lateral pilot performance.**

## Nomenclature

| | | |
|---|---|---|
| $dt$ | = | fast-time simulation time step, s |
| $e_{ss}$ | = | steady-state error |
| $g_0$ | = | gravitational acceleration, m/s$^2$ |
| $N$ | = | unit normal |
| $n_z$ | = | vertical load factor |
| $p, q, r$ | = | roll rate, pitch rate, yaw rate, deg/s |
| $R$ | = | radius, m |
| $T_{fts}$ | = | fast-time simulation computation horizon, s |
| $\boldsymbol{V}_a$ | = | aerodynamic velocity, m/s |
| $\boldsymbol{V}_k$ | = | kinematic (Earth-fixed) velocity, m/s |
| $V_{TAS}$ | = | true airspeed, m/s |
| $\boldsymbol{V}_w$ | = | wind velocity, m/s |
| $x_e, v_e$ | = | lateral, vertical position error, m |
| $\beta$ | = | slip angle, deg |
| $\gamma_a$ | = | aerodynamic flight-path angle, deg |
| $\gamma_e$ | = | climb-angle error, deg |
| $\gamma_k$ | = | kinematic flight-path angle, deg |
| $\Delta T$ | = | flight-path vector-oriented FBW time lag, s |
| $\Delta X$ | = | angular distance, m |
| $\delta_{e_s}, \delta_{a_s}$ | = | elevator, aileron stick displacements, deg |
| $\delta_{e_c}, \delta_{a_c}$ | = | elevator, aileron control surface deflections, deg |
| $\theta, \phi, \psi$ | = | pitch, roll, yaw attitude angle, deg |
| $\kappa$ | = | curvature, m$^{-1}$ |
| $\xi$ | = | crab angle, deg |
| $\tau_{ss}$ | = | time at steady-state error, s |
| $\chi_a$ | = | heading angle, deg |
| $\chi_e$ | = | track-angle error, deg |
| $\chi_k$ | = | course/track angle, deg |
| $\chi_w, \gamma_w$ | = | wind azimuth, elevation angle, deg |

Presented as Paper 2004-5236 at the AIAA Guidance, Navigation, and Control Conference, Providence, RI, 16–19 August 2004; received 7 March 2005; revision received 4 June 2005; accepted for publication 18 July 2005. 

*Research Associate, Control and Simulation Division, Faculty of Aerospace Engineering, Kluyverweg 1, 2629 HS Delft, The Netherlands; c.borst@lr.tudelft.nl.

†Assistant Professor, Control and Simulation Division, Faculty of Aerospace Engineering, Kluyverweg 1, 2629 HS Delft, The Netherlands; m.mulder@lr. tudelft.nl. Member AIAA.

‡Associate Professor, Control and Simulation Division, Faculty of Aerospace Engineering, Kluyverweg 1, 2629 HS Delft, The Netherlands; m.m.vanpaassen@lr.tudelft.nl. Member AIAA.

§Professor, Chairman of the Control and Simulation Division, Faculty of Aerospace Engineering, Kluyverweg 1, 2629 HS Delft, The Netherlands; j.a.mulder@lr.tudelft.nl. Member AIAA.

## I. Introduction

SINCE the introduction of perspective flight-path displays such as the "tunnel in the sky" and "highway in the sky," much research has been conducted to improve pilot path-following performance with these displays when flying complex curved trajectories. Two common techniques to enhance performance are display augmentation, in which the display is augmented with additional symbols,[1–7] and control augmentation, in which the inner loops of the aircraft control task are automated by a control augmentation system (CAS).[8–14]

Two well-known display-augmentation techniques are the flight-path vector (FPV) and flight-path predictor (FPP).[1–3,5,6,15] The FPV shows the aircraft ground-referenced (or inertial) direction of motion, whereas the FPP shows the aircraft future position some seconds ahead in time with respect to a predictor reference frame moving ahead of the aircraft in the tunnel.

A promising control augmentation concept is flight-path oriented control, which allows the pilot to directly control the ground-referenced aircraft direction of motion.[11,13] Its design is based on the "velocity vector control wheel steering and display system," or "velocity CWS," developed by Boeing and NASA in the 1970s and 1980s.[8,9,16–21]

A comparative study between flight-path predictor display augmentation and flight-path-oriented control augmentation showed that the FPP yielded the best position-tracking performance, whereas the control augmentation resulted in superior flight-path-tracking performance, the lowest control activity, the lowest pilot workload, and a more comfortable ride.[14,22] The flight-path-oriented control augmentation was concluded to be superior in flying straight sections of the trajectory but less suitable for following curved sections.[14] This is because in a turn the aircraft flight path relative to the ground must change continuously, and because the control law interpreted the lateral stick deflection as a track-angle rate command, pilots had to keep the stick deflected while tracking curves. Although pilots soon settled for this solution, similar to the situation in automobile driving, they did not appreciate it. Furthermore, it was unclear what stick deflection was needed to command the correct track-angle rate.

Clearly, lateral maneuvers with a flight-path command control law raise several issues. A possible solution would be to have the pilot command the curvature rate of the aircraft trajectory instead of the track-angle rate. But besides designing a different control architecture, this would also require a different visualization on the display to show the pilots the effects of the curvature-rate command on the future aircraft trajectory. This led to the design of a path-oriented control and display-augmentation concept in which the pilot directly commands the aircraft's future trajectory.

This paper presents the path-oriented augmentation concept. It is structured as follows. First, the findings of earlier investigations on the flight-path control augmentation are discussed briefly. Then, the control architecture and implementation details of the path-oriented control and display augmentation are presented, together with findings of offline simulations. Finally, the results of a pilot-in-the-loop experiment, conducted in a fixed-base simulator, are discussed. The goal of this experiment was to study pilot performance and workload with the new path-oriented display and control-augmentation system as compared to more conventional display and control-augmentation concepts.

## II. Shortcomings of the Current Flight-Path-Oriented Control Augmentation

For a detailed analysis of the benefits of display and control-augmentation concepts in perspective flight-path displays, the reader is referred to previous papers on this subject.[11–14,22,23] Only the main findings for the flight-path control augmentation are discussed in the following.

In control augmentation, the inner loops of the pilot's guidance task are closed by a fly-by-wire control system, allowing the pilot to directly manipulate aircraft states higher in the control hierarchy. In particular flight-path oriented control is considered to be a promising concept.[8–14,16–21] Here, the pilot directly commands the aircraft ground-referenced direction of motion, that is, the flight-path vector. It is generally implemented as, in the lateral dimension, a track-angle rate command/track-angle hold system, and in the longitudinal dimension, a climb-angle rate command/ climb-angle hold system. The current flight-path vector and the commanded flight-path vector are shown as two separate FPV symbols on the display.[8,16,17,20,24–27]

Previous work showed that the primary advantage of the flight-path oriented control augmentation is that it relieves pilots from compensating for atmospheric disturbances acting on the aircraft, allowing them to concentrate on the "where-to-go" loop.[13] This reduces workload and control activity significantly, at similar or better levels of path-following performance as compared to the more conventional display-augmentation concepts such as the flight-path predictor.[14]

Although promising, flight-path vector-control augmentation has some disadvantages that need to be resolved. These are discussed briefly in the following.[14]

### A. Constant Stick Deflections During Turns

In the present implementation of the lateral flight-path vector-control law, the side stick lateral displacement is proportional to the commanded track-angle rate $\dot{\chi}_k^c$. This implies that the pilot must give a constant stick input to the left (right) in left (right) turns. Previous experiments indicated that although pilots quickly adapted to the new control strategy, they did not approve it.[13,14]

Lam et al.[14,22] recommended circumventing this problem by interpreting the lateral stick deflection as a track-angle rate-rate command, that is, a curvature-rate command. However, this would require a different visualization on the display. For a pilot to accurately control the trajectory curvature, the flight-path vector command symbol does not satisfy, because it only shows the tangent to the aircraft trajectory. This recommendation is dealt with later in the path-oriented augmentation concept.

### B. Lagged Response of the Control Law

The open-loop combination of the FBW control law and the aircraft dynamics is a type 1 system[28,29] for the response in track angle to the commanded track angle $\chi_k^c$. In straight flight, with a constant $\chi_k^c$, the steady-state error will thus be zero, but the system will experience a "velocity error" in a curve, when $\chi_k^c$ is linearly increasing. The pilot experiences this as a lagged response of the control law. Lam[14] showed that this time lag $\Delta T$ depends on the aircraft velocity and the bandwidth of the controller. The lag affects performance and because pilots are likely to compensate for it, this may contribute to workload. Figure 1 shows the situation from above, illustrating that it takes $\Delta T$ s before the aircraft track angle $\chi_k$ equals the commanded track angle $\chi_k^c$.

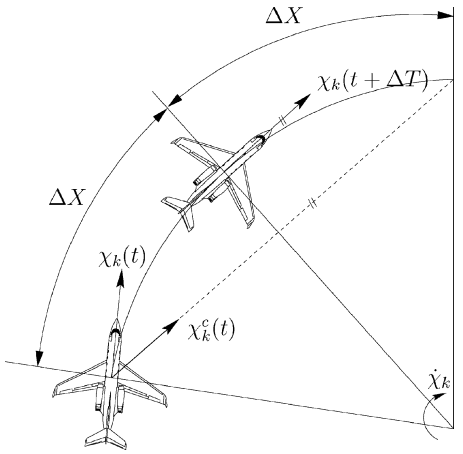


**Fig. 1 Top view of the angular distance $\Delta X = \Delta T \cdot V$ in which the aircraft track angle $\chi_k$ reaches the commanded track angle $\chi_k^c$ issued at time $t$ [i.e., $\chi_k(t+\Delta T) = \chi_k^c(t)$].**

### C. Lack of a Reference for the (Commanded) Flight-Path Vector

Previous implementations of the flight-path control augmentation lacked a reference that the pilots could use to aim the commanded flight-path vector.[13] Especially in turns pilots had difficulty estimating where to put the FPV command symbol to accurately track the reference trajectory. Lam suggested showing a reference frame moving ahead of the aircraft in the tunnel wireframe, similar to the FPP concept.[14]

Two possibilities exist for including this reference frame on the display (see Fig. 1). First, one could put the reference frame at an angular distance $\Delta X$ ahead, corresponding with $\Delta T$. This frame then shows where in the tunnel ahead the aircraft track angle $\chi_k$ will have reached the track $\chi_k^c(t)$ commanded at that moment in time. An experimental evaluation of this possibility showed that pilot performance improved, with slightly higher pilot workload and control activity. Pilots commented, however, that the reference frame was flying too close ahead to be useful.[14]

The second option is to put the reference frame at an angular distance ahead that is twice as large, that is, at $2 \cdot \Delta X$. The frame can then act as a target: putting the commanded FPV in its center would result in the right aircraft track angle $\Delta T$ later in time (see Fig. 1). A pursuit-tracking task results that is similar to the flight-path predictor display augmentation, but now combined with the control augmentation. This solution represents the best of two worlds and is therefore included as one of the augmentation-concept candidates evaluated in the experiment described here.

## III. Path-Oriented Control and Display Augmentation

### A. Concept

The two main design requirements for the path-oriented control and display-augmentation concept were, first, to enable an aircraft to accurately fly circular curved ground-referenced trajectories, irrespective of crosswinds, and second, to relieve the pilot from holding the side stick deflected during turns. Note that the velocity CWS introduced already contained a "curved track" command capability that enabled the aircraft to execute an exact circular ground track, regardless of wind. The pilot commanded a turn radius while a bank-angle command was adjusted automatically by the ground speed to compensate for crosswinds.[8]

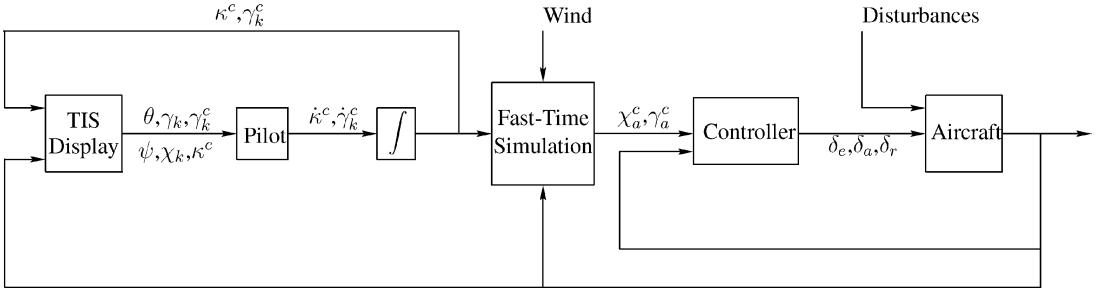


**Fig. 2 Schematic block diagram of the path-oriented control augmentation.**

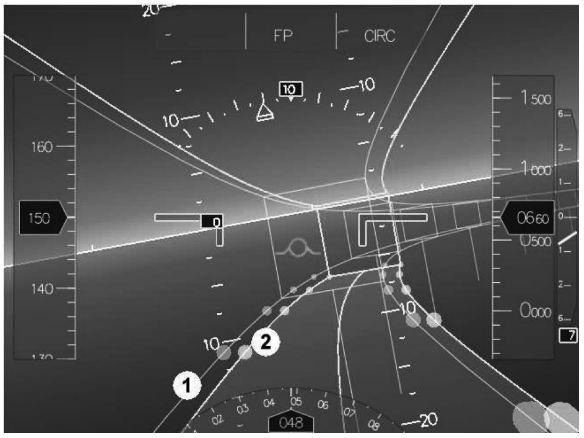


**Fig. 3 Tunnel display augmented with the command tunnel. In this figure, 1 depicts the reference tunnel and 2 depicts the command tunnel.**

Here a different approach was taken: through moving the stick, pilots command the curvature-rate of the future aircraft trajectory, which is shown on the tunnel display a few of seconds ahead. Then, because the tunnel nominal trajectory is usually a concatenation of straight and circular segments, the command trajectory can be shaped similarly into straight (infinite-curve radius) or circular (finite-curve radius) paths.

To have the aircraft follow the commanded trajectory, a fast-time simulation (FTS) system interprets the pilot stick deflections as curvature-rate/climb-angle rate commands and computes, in real time, wind-compensated reference signals that are then tracked by a control-augmentation system. A schematic block diagram is shown in Fig. 2. In the Appendix all the reference frames and some important relationships are defined, which are used throughout this paper.

### B. Tunnel Display Augmentation

The tunnel-in-the-sky display will be augmented with a command tunnel representing a three-dimensional analog of the future trajectory that will be flown (see Fig. 3). The command tunnel always starts at the aircraft's center of gravity. The width and height of the command tunnel equal the dimensions of the reference tunnel such that the pilot can immediately perceive the deviation of the command tunnel with the reference tunnel. The length of the command tunnel centerline is computed in flight by integrating the groundspeed of the aircraft along the commanded curve for a number of $T_{\text{fts}}$ s.

### C. Pilot Control Task

The control task of the pilot is a pursuit-tracking task with preview, in which the pilot has to align the shape of the future (command) trajectory with that of the reference tunnel trajectory to follow the latter. As far as the pilot is concerned, longitudinal side stick deflections are interpreted as climb-angle rate ($\dot{\gamma}_k^c$), climb-angle hold commands (similar to earlier concepts[8,11,12,22]). Lateral side stick deflections are interpreted as curvature rate ($\dot{\kappa}^c$), curvature hold commands. By controlling the rates of the command signals it is ensured that when the stick is in its neutral position, the current climb angle and curvature are held constant.

### D. Fast-Time Simulation Algorithm

The FTS algorithm is responsible for computing the set points of the flight-control system from the commanded curvature ($\kappa^c$) and the kinematic (Earth-fixed) flight-path angle $\gamma_k^c$ (see Fig. 2). The set points of the flight-control system are the aerodynamic flight-path angle $\gamma_a$ and heading angle $\chi_a$ computed along the commanded kinematic curved flight path. Thus, the FTS algorithm needs to compute the command signals for the control system $T_{\text{fts}}$ s ahead in time. The computation of the command signals is done in three stages.

*Stage 1:* Collect the current aircraft attitude and velocity, the wind magnitude and direction, and the pilot command signals ($\gamma_k^c$ and $\kappa^c$).

*Stage 2:* Simulate the aircraft motion along commanded the kinematic flight path for $T_{\text{fts}}$ s and compensate for crosswinds to calculate aerodynamic set points.

*Stage 3:* Pass the aerodynamic controller set points along the commanded kinematic flight path to the flight-control system.

Stages 1–3 are repeated every simulation time step to update for altered pilot-controlled command data and changed wind data. A more detailed description of each stage is discussed in the following.

#### 1. Stage 1

The FTS system measures the stick deflection, the aircraft data (kinematic flight path $\chi_k$, $\gamma_k$, kinematic track-angle rate $\dot{\chi}_k$, and true airspeed $V_{\text{TAS}}$) and wind information (magnitude $V_w$, direction $\chi_w$, $\gamma_w$) to initialize the FTS algorithm. The required data is then as follows:

Side stick: $\kappa^c$ and $\gamma_k^c$.

Aircraft: $\chi_k$, $\dot{\chi}_k$, $\gamma_k$, and $V_{\text{TAS}}$.

Wind: $V_w$, $\chi_w$, and $\gamma_w$.

Note that the algorithm does not need the aircraft's position relative to the Earth for initialization, because the command signals sent to the flight-control system are directions and the future trajectory always starts at the aircraft's center of gravity.

#### 2. Stage 2

The aircraft's kinematic Earth-fixed velocity vector is calculated and placed tangential to the commanded kinematic trajectory. In the FTS loop the aerodynamic set points ($\chi_a^c$ and $\gamma_a^c$) are computed at each FTS time step and stored in arrays. These arrays hold the commanded heading and aerodynamic flight-path angles at each time step along the commanded kinematic trajectory. In this algorithm the dynamics of the aircraft are not taken into account. Instead, the algorithm is entirely based on the kinematic relations between the aerodynamic velocity $\boldsymbol{V}_a$ and kinematic velocity $\boldsymbol{V}_k$ in the presence of crosswind. On a pseudo-programming level, the steps of the FTS loop at this stage are as follows.

*Step 1:* Store the measured aircraft data and initialize the FTS loop.

*Step 2:* Compute at the current FTS time step $\chi_a$, $\gamma_a$, and $V_k$ from the measured wind magnitude and direction, true airspeed, and known course angle.

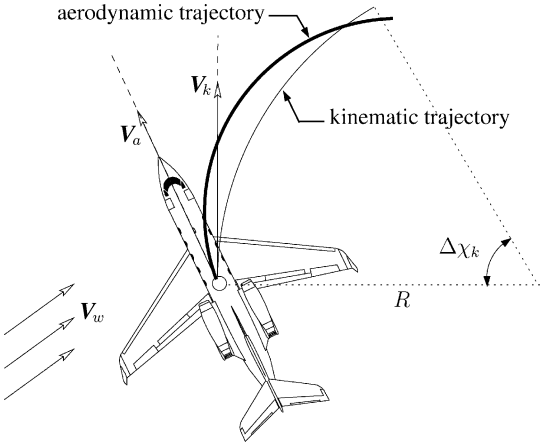


**Fig. 4 FTS system converts the commanded future kinematic (Earth-fixed) trajectory into a future aerodynamic trajectory based on wind information.**

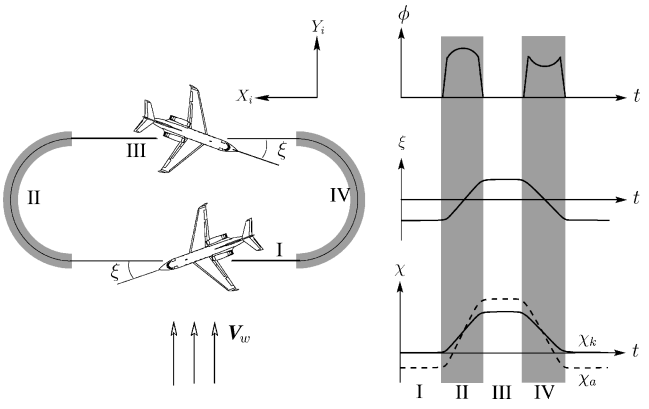


**Fig. 5 To follow circular segments relative to the Earth, a pilot should continuously change the aircraft roll angle $\phi$ and crab angle $\xi$, in a nonlinear fashion.**

*Step 3:* Calculate the course angle $\chi_k$ at the next FTS time step using the fact that the aircraft is supposed to move along a circular trajectory. Numerically, the course angle at the next FTS time step is calculated as follows:

$$\chi_{k_{i+1}} = \chi_{k_i} + \left(V_{k_i} \cdot \kappa^c\right) \mathrm{d}t \tag{1}$$

In Eq. (1) it is clearly seen that the incremental course angle is calculated with the rotational velocity of the kinematic speed tangential to a circular path.

*Step 4:* Update the initial conditions of the FTS loop to their new values.

Steps 1–4 are repeated until the loop time has reached $T_{\text{fts}}$ s.

In essence, the FTS system converts the commanded kinematic trajectory into an aerodynamic trajectory (see Fig. 4). Why this is necessary can be explained as follows.

In nonzero wind, guiding an aircraft along straight sections of an Earth-fixed trajectory is not a difficult task. The deviation from the desired heading indicates the influence of the wind and, by regularly scanning the heading indicator, the pilot can compensate for the wind by adopting a certain crab angle $\xi$ (see Fig. 5). The result is that the wind carries the aircraft along the Earth-fixed trajectory as seen from an observer on the ground. However, during curved trajectories the heading is continuously changing, meaning that the heading indicator cannot be used for wind compensation. Because the aircraft is carried by the wind, flying circular trajectories requires a continuous change in aircraft roll angle $\phi$ and crab angle $\xi$ that is completely dependent on the wind velocity and direction. An offline analysis of the angles between the reference frames showed that the roll angle and crab angle should change in a nonlinear fashion to stay on the circular Earth-fixed trajectory (see Fig. 5). Flight tests with the tunnel display indeed showed that pilots have great difficulty in performing this task unaided, at least with the high accuracy levels as required by the tunnel display. A thorough discussion about the desired tracking performance and accuracy levels required by the tunnel can be found in earlier research conducted by the Control and Simulation division.[13,30,31]

Therefore, in step 2 of the FTS algorithm the aerodynamic set points are calculated to relieve the pilot from having to compensate for crosswinds. Converting those aerodynamic set points from the kinematic command variables (see Fig. 2) can be done as follows.

The commanded trajectory is known in terms of curvature and elevation. Hence, the desired direction of the kinematic velocity is also known in advance, because the kinematic velocity is tangential to this Earth-fixed command trajectory. In a steady atmosphere, it is acceptable to assume that the wind velocity is constant in magnitude and direction over a small period of time. Additionally, the airspeed can also be considered constant over a small period of time. These assumptions allow the aerodynamic angles $\chi_a$ and $\gamma_a$ to be calculated using basic vector operations and properties.

First, the unknown components of the aerodynamic velocity relative to the inertial reference frame are defined as follows:

$$\boldsymbol{V}_a = [u_a \quad v_a \quad w_a]^T \tag{2}$$

Second, it is known that $\boldsymbol{V}_k$ lies along the $X_k$-axis of the kinematic reference frame,[32] thus in the direction of unity vector $\boldsymbol{n}_{kx}$ along the $X_k$-axis. Hence, the unity vectors $\boldsymbol{n}_{ky}$ and $\boldsymbol{n}_{kz}$ along the $Y_k$-axis and $Z_k$-axis, respectively, are perpendicular to the kinematic velocity. The kinematic velocity itself is the vector sum of the wind velocity and aerodynamic velocity [see Eq. (11)]. Therefore, the following properties are valid:

$$(\boldsymbol{V}_a + \boldsymbol{V}_w) \cdot \boldsymbol{n}_{ky} = 0 \tag{3a}$$

$$(\boldsymbol{V}_a + \boldsymbol{V}_w) \cdot \boldsymbol{n}_{kz} = 0 \tag{3b}$$

Writing all vectors in Eqs. (3a) and (3b) with respect to the inertial reference frame yields two equations with three unknowns, that is, the components of $\boldsymbol{V}_a$. Therefore an extra equation is needed containing the components of $\boldsymbol{V}_a$. This equation is the inner product of $\boldsymbol{V}_a$ with itself, hence

$$\boldsymbol{V}_a \cdot \boldsymbol{V}_a = \|\boldsymbol{V}_a\|^2 = V_a^2 \tag{4}$$

Now the quadratic Eq. (4) has to be solved using Eqs. (3a) and (3b). Solving the quadratic equation will yield two solutions. Thus two possible vectors for $\boldsymbol{V}_a$ can be constructed, but only one of them is the correct solution. To filter out the correct solution, vector $\boldsymbol{n}_{kx}$ will be used. Because it is known that $\boldsymbol{V}_a$ is directed forward and $\boldsymbol{n}_{kx}$ is also directed forward, the inner product of these two vectors must be positive (see Fig. 6). Hence the correct solution must hold the following property:

$$\boldsymbol{V}_a \cdot \boldsymbol{n}_{kx} > 0 \tag{5}$$

Before solving the quadratic Eq. (4), all vectors used in Eqs. (3a), (3b), (4), and (5) have to be expressed in the same reference frame (i.e., the inertial reference frame).

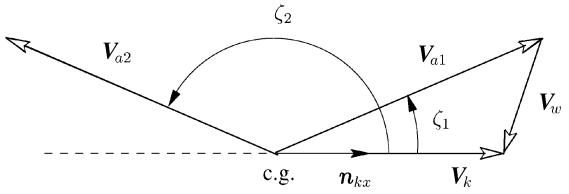


**Fig. 6 Solving the quadratic equation (4) yields two solutions: $V_{a1}$ and $V_{a2}$. Only the aerodynamic velocity vector $V_{a1}$ in the direction of the kinematic velocity (yielding a positive inner product) is the correct solution.**

After solving the quadratic equation, the aerodynamic angles $\chi_a$ and $\gamma_a$ can be determined by transforming the aerodynamic velocity from the aerodynamic reference frame to the inertial reference frame.[32]

$$\gamma_a = -\arcsin(w_a/V_a) \tag{6a}$$

$$\chi_a = \arccos(u_a/V_a \cos\gamma_a) \tag{6b}$$

*3. Stage 3*

The aerodynamic command signals will be passed to the flight-control system.

*4. Considering Aircraft Limitations*

The FTS algorithm contains a function to limit the curvature of the commanded trajectory, because a too-large curvature (or too-small radius) would require unacceptably large roll angles and high load factors. The maximum roll angle is set to $|\phi_{\max}| = 30$ deg. Assuming that the aircraft is coordinated, the roll angle can be calculated as follows[7,8]:

$$\phi = \arctan\left(V_k^2 \big/ g_0 R\right) \tag{7}$$

The maximum roll angle is used with Eq. (7) to limit the commanded curvature:

$$|\kappa_{\max}| = \left(g_0 \tan|\phi_{\max}| \big/ V_k^2\right)\left(= |R_{\min}|^{-1}\right) \tag{8}$$

Besides the maximum curvature, the minimum curvature should also be considered. By commanding a curvature less or equal than the minimum curvature, the system assumes that the pilot wants to fly straight ahead. To prevent the aircraft from rolling when the minimum curvature is reached, the FTS algorithm must keep the commanded heading angle constant. The minimum curvature is set to $|\kappa_{\min}| = 0.00002$ (or $|R_{\max}| = 50 \cdot 10^3$ m).

### E. Control Laws

The flight-control laws are based on classical multiloop hold/select modes of an autopilot[33,34] and automate the inner loops of the pilot control task.

*1. Longitudinal Control Law*

The longitudinal control law is a climb-mode (CM) control law that tracks the commanded aerodynamic flight-path angle $\gamma_a^c$. Essentially, the CM controller controls the climb/descent speed of the aircraft ($\dot{h} = V_a \sin\gamma_a$) and uses a classical pitch-attitude hold (PAH) controller as inner loop. For making steady-state turns, turn compensation is used in the design of the CM control law based on the following equation[34]:

$$q = r \tan\phi \tag{9}$$

where $q$ and $r$ represent the aircraft pitch and yaw rates, respectively. The CM control law with turn compensation is shown in Fig. 7a.

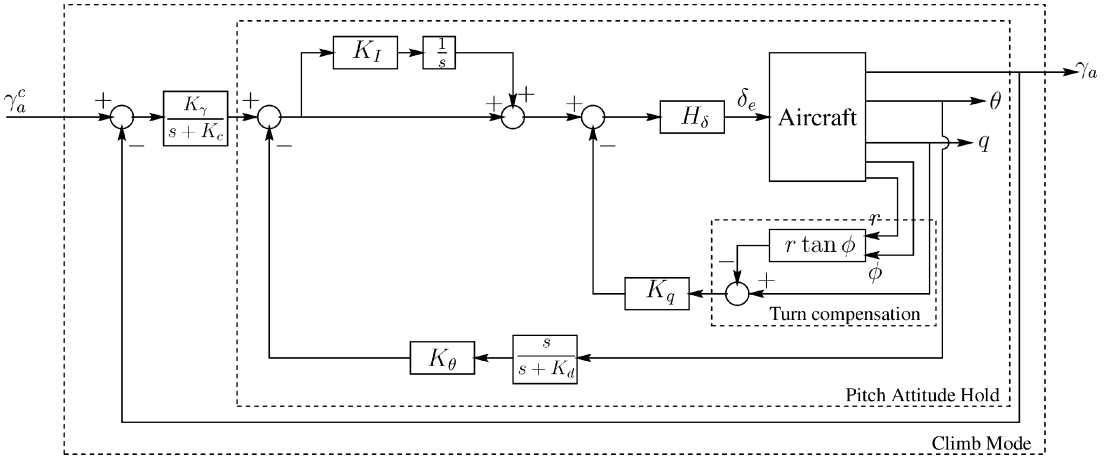


**a) Climb-mode control law with turn compensation**

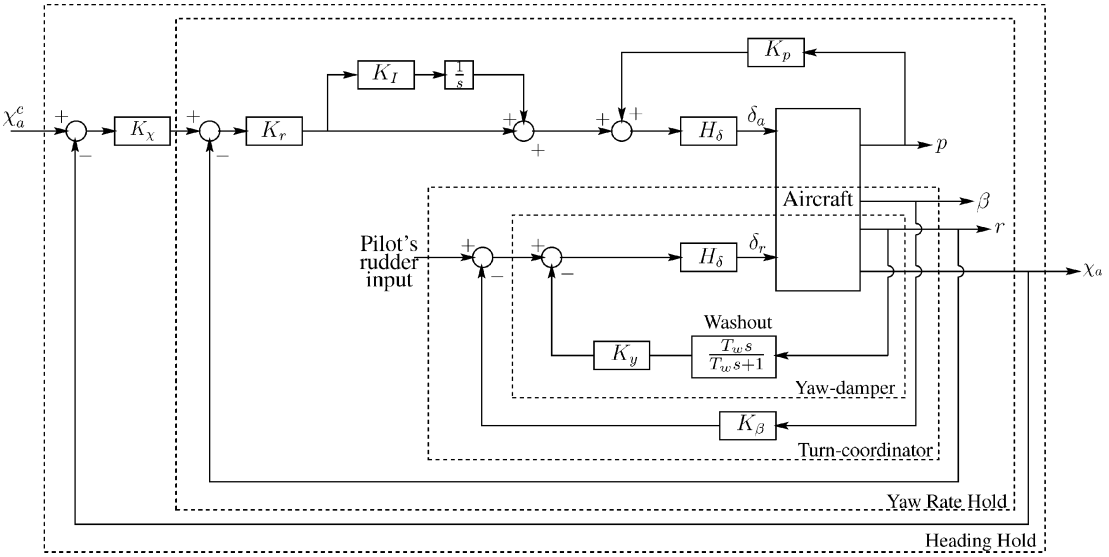


**b) Heading-hold control law with turn coordinator and yaw damper**

**Fig. 7 Longitudinal control law (climb mode) and lateral control law (heading hold).**

*2. Lateral Control Law*

The lateral control law consists of a heading-hold (HH) control law with a yaw-damper stability-augmentation system for damping the Dutch roll, and a turn coordinator for minimizing the sideslip angle $\beta$. The inner loop of the HH control law is a yaw-rate hold (YRH) control law, which maintains a certain commanded yaw rate of the aircraft. The block diagram of the HH control law is depicted in Fig. 7b.

*3. Auto-throttle*

The control systems described only work properly if the airspeed remains constant. For this purpose an auto-throttle is used, a simple control law that deflects the throttle to keep the difference between the actual and desired airspeed within approximately 5 kn.

### F. Velocity Steady-State Error Compensation

To be useful for following circular curved trajectories, the lateral control law of the path-oriented control augmentation must at least be able to track a ramped heading command signal. Otherwise the aircraft will never be able to follow the commanded curve. The integrator in the feed-forward path of the HH control law, Figure 7b, ensures that the system's response has a zero steady-state error for a step input. However, it cannot follow a ramp without having a constant velocity steady-state error.[28,29] To follow a ramp it would be necessary to cascade the integrator in the feed-forward path with an additional integrator. However, this has a negative effect on the performance and, most important, the stability of the closed-loop system.[29]

Compensating for the constant velocity steady-state error without introducing an additional integrator is done as follows. First, the velocity steady-state error $e_{ss}$ is determined by subtracting the (steady-state) closed-loop system's response, due to a unit-ramp command $\chi_a^c(t) = t$, with the unit-ramp command (Fig. 8a). Because the input is unit ramp, the value of the steady-state error $e_{ss}$ equals the time $\tau_{ss}$ at which the unit ramp has a value of $e_{ss}$. Second, the constant $\chi_a^c(t = \tau_{ss})$ will be added to the unit-ramp input, yielding the signal $\hat{\chi}_a^c(t)$:

$$\hat{\chi}_a^c(t) = \chi_a^c(t) + \chi_a^c(\tau_{ss}) \tag{10}$$

Examining the closed-loop system response resulting from input $\hat{\chi}_a^c(t)$ clearly shows that the required command signal $\chi_a^c(t)$ will now be tracked without having a velocity steady-state error (see Fig. 8b).

Offline simulation analysis indicated that Eq. (10) also applied for ramp command signals with arbitrary slopes, in which the constant $\tau_{ss}$ was determined by tracking a unit-ramp command. How aircraft type and configuration influence $\tau_{ss}$ was unclear, however, and required more investigation. Note that velocity steady-state error compensation is not needed for the longitudinal control law, because its input will only be subjected to discrete flight-path changes.

In this paper a six-degree-of-freedom (DOF) nonlinear model of the Cessna Citation 500 is used,[35] trimmed at an altitude of 2000 ft, flight-path angle of $\gamma_k = -3$ deg, and a true airspeed of $V_a = 150$ kn (77.16 m/s) with 15-deg flaps. For this aircraft and configuration, the gains of the CM and HH control laws are listed in Table 1.

Furthermore, this operating point resulted in $\tau_{ss} = 1.523$ s for obtaining a zero velocity steady-state error. In Fig. 9 the influence of off-design operating points on $\tau_{ss}$ is investigated. From this figure it can be seen that the altitude does not affect $\tau_{ss}$. The true airspeed has only a small effect on $\tau_{ss}$: for airspeeds other than the trim condition for which the controller gains were designed, $\tau_{ss}$ will decrease very slightly (i.e., 0.017% at $V_{TAS} = 200$ kn (102.89 m/s)). For the experiments discussed in the next section, the effect of $V_{TAS}$ on $\tau_{ss}$ is not relevant at all, because the airspeed will be held constant by means of an auto-throttle system.

In Fig. 10 some relevant aircraft responses are provided that show responses with and without compensating for the steady-state error. From this figure it can be seen that applying the compensation highly improves the path-following performance. The flight-control system is indeed capable of very accurately tracking a commanded circular ground-referenced trajectory in the presence of a strong crosswind. For the pilot-in-the-loop experiment discussed later, the velocity steady-state error compensation will be implemented in the FTS system.

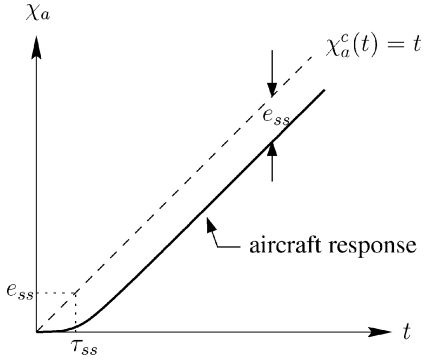


**a) Tracking $\chi_a^c$**

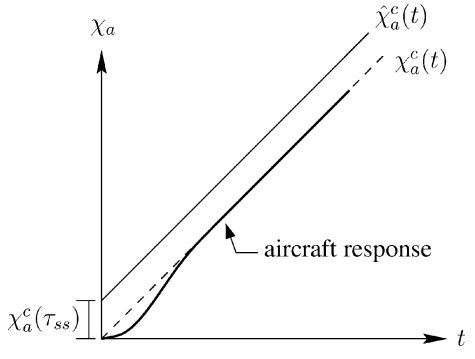


**b) Tracking $\hat{\chi}_a^c$**

**Fig. 8 Tracking command signal $\hat{\chi}_a^c(t)$ will result in following the desired signal $\chi_a^c(t)$.**

**Table 1 Gains of the CM, HH, and yaw damper/turn coordinator for the following trim condition of the Cessna Citation I: $V_{TAS} = 150$ kn, $h = 2000$ ft, $\gamma_k = -3$ deg, and flaps APP (15 deg)**

| Longitudinal | | Lateral | | | |
|---|---|---|---|---|---|
| CM | | HH | | Rudder control | |
| Parameter | Value | Parameter | Value | Parameter | Value |
| $K_\gamma$ | −0.1600 | $K_\chi$ | 0.7300 | $K_y$ | 2.0000 |
| $K_c$ | 0.2000 | $K_I$ | 4.3500 | $T_w$ | 4.0000 |
| $K_I$ | 2.0000 | $K_\phi$ | 0.3100 | $K_\beta$ | 10.0000 |
| $K_q$ | −0.0800 | $K_p$ | 0.0060 | | |
| $K_\theta$ | −0.3100 | $K_r$ | −0.0115 | | |
| $K_d$ | 0.2000 | | | | |

## IV. Experiment

The goal of the experiment was to test the usefulness of the path-oriented control augmentation in conjunction with a tunnel-in-the-sky display, and compare it with other display and control-augmentation concepts in terms of pilot performance, control activity, and workload.

### A. Method

*1. Subjects and Instruction to Subjects*

Six subjects, all professional pilots, participated in the experiment, with an average of 4300 flying hours (Table 2). The subjects were instructed to control the aircraft along the reference trajectory as accurately as possible.

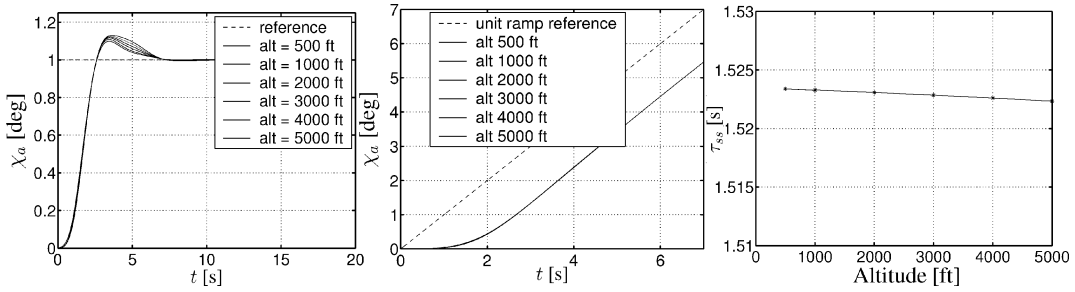


**a) Lateral aircraft response to unit step and unit ramp inputs, and $\tau_{ss}$ vs altitude**

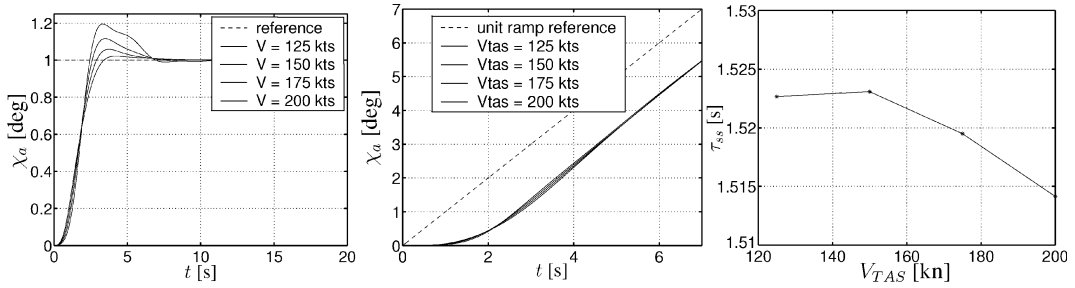


**b) Lateral aircraft response to unit step and unit ramp inputs, and $\tau_{ss}$ vs true airspeed**

**Fig. 9 Lateral aircraft responses and $\tau_{ss}$ as functions of altitude and true airspeed initial conditions, while tracking a unit step and ramp reference signal. The design operating point for the control laws is at an airspeed $V_{TAS}$ = 150 kn and an altitude of 2000 ft.**

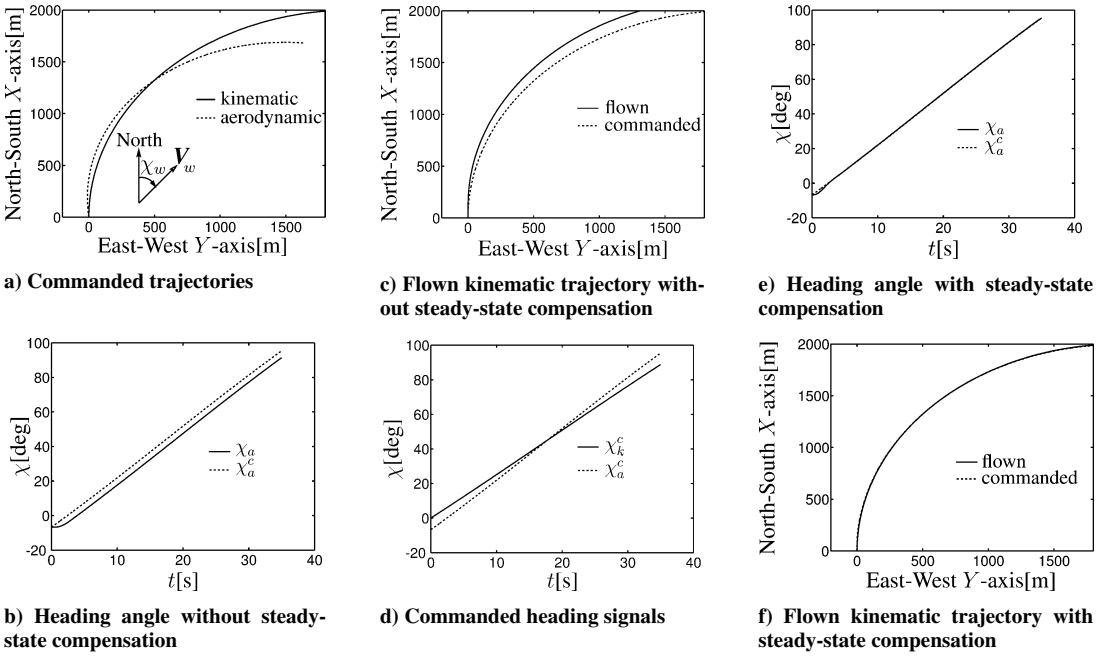


**a) Commanded trajectories**

**c) Flown kinematic trajectory without steady-state compensation**

**e) Heading angle with steady-state compensation**

**b) Heading angle without steady-state compensation**

**d) Commanded heading signals**

**f) Flown kinematic trajectory with steady-state compensation**

**Fig. 10 Aircraft responses with and without steady-state compensation. A circular kinematic trajectory is followed with a radius of $R$ = 2000 m for 35 s. The wind magnitude was $V_w$ = 25 kn with a heading of $\chi_w$ = 45 deg.**

**Table 2 Characteristics of the pilot subjects in the experiment**

| Pilot | Age | Hours | Types of aircraft |
|---|---|---|---|
| A | 31 | 1,900 | single-engine, B747-400 |
| B | 64 | 13,000 | single-engine, Cessna Citation II, DC3, DC8, B747-200/300/400 |
| C | 28 | 4,100 | single-engine, Beech 99/King Air, Metro III, B747/767 |
| D | 28 | 831 | single-engine, Cessna 150/152/172, B737-300/400, B747-300 |
| E | 28 | 340 | single-engine, B737-300/700 |
| F | 37 | 5,652 | single-engine, Cessna C500, B747-400, B767, B777 |

*2. Apparatus*

A fixed-base flight simulator was used. The tunnel display was presented on a 18-in. LCD screen 0.80 m in front of the pilot. The control manipulators were an electrohydraulic side stick and rudder pedals, both simulated with normal (i.e., passive) characteristics. An outside visual was projected onto a wall in front of the cockpit mockup.

*3. Independent Variables*

Two independent variables were manipulated in the experiment: four augmentation concepts (AC) and two wind conditions (WC).

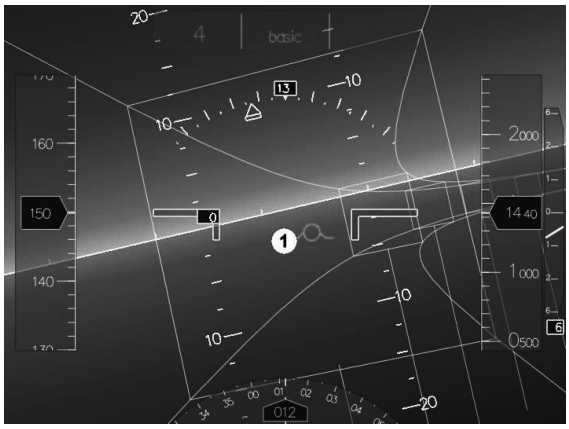

a) FPV: Baseline control, with 1, FPV symbol

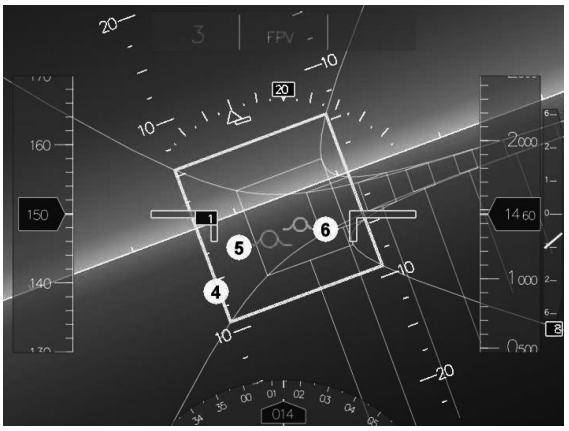

c) FBW: Flight-path vector oriented control augmentation, with 4, command FPV reference frame: 5, true FPV, and 6, commanded FPV

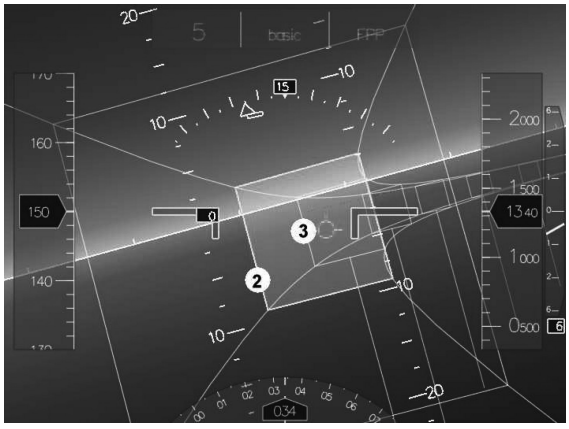

b) FPP: Flight-path vector display augmentation, with 2, predictor reference frame and 3, FPP symbol

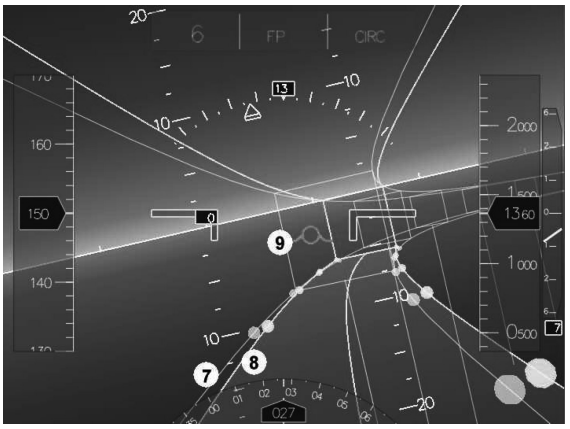

d) FBW+: Path-oriented control augmentation, with 7, reference tunnel: 8, command tunnel; and 9, true FPV

**Fig. 11 Augmentation concepts used in the experiment.**

The augmentation concepts were as follows:

1. *Baseline control with FPV display augmentation* (FPV), that is, the unaugmented control of the aircraft using elevator, aileron, and rudder deflections directly coupled to the side stick and pedals. A green FPV symbol is presented (Fig. 11a). This concept represents our baseline.

2. *Flight-path predictor display augmentation* (FPP), that is, the direct-link manual control, but now a green flight-path predictor is presented together with a yellow transparent predictor reference frame, moving a fixed time $T_p$ ahead in the tunnel (Fig. 11b). The "optimal prediction time" was found to be 3 s.[14] This concept represents the "tunnel-and-predictor" concept that is widely used in perspective flight-path displays.

3. *Flight-path oriented FBW control/display augmentation* (FBW), in which the pilot commands the kinematic direction of the aircraft motion. The pilot stick deflections are interpreted by the FBW computer as climb-angle rate and track-angle rate commands. A green FPV symbol shows the instantaneous direction of motion and a yellow FPV symbol shows the commanded direction of motion. A yellow transparent FPV command reference frame is presented at $2\Delta T$ s ahead in the tunnel (Fig. 11c). Pointing the command FPV in the middle of the reference frame results in the aircraft having the right track angle $\Delta T$ s ahead.

4. *Path-oriented FBW control/display augmentation* (FBW+), in which the pilot commands the future trajectory of the aircraft as explained in the previous section. Nonzero side stick deflections are interpreted by the FBW computer as a curvature-rate command (lateral) and a climb-angle rate command (vertical). The FTS algorithm had a computation horizon $T_{\text{fts}}$ of 7.0 s, which was determined by offline simulations.

The future commanded trajectory is shown in three-dimensional perspective as a command tunnel (see Fig. 11d), with the same size as the tunnel depicting the nominal trajectory. The boundaries of the command tunnel ground plane were augmented with support points in the form of small spheres. By also displaying their projections on the reference tunnel boundaries, the pilot had to match the spheres to follow the reference tunnel.

In all control systems the side slip was minimized automatically; the rudder pedals were not needed. The aircraft aerodynamic velocity was automatically held at 150 kn indicated air speed (IAS) through an auto-throttle.

The two wind conditions were normal wind (8 kn at 1000 ft) and heavy wind (30 kn at 1000 ft). Both winds decreased with altitude and were constant in direction. Atmospheric turbulence was not simulated.

### *4. Experiment Design*

A factorial within subjects design was used, yielding eight conditions (4 AC $\times$ 2 WC). The trajectory was mirrored with respect to a fictituous localizer plane to prevent pilot boredom and also to prevent them from performing the task by rote.

### *5. Procedure*

Each pilot performed four blocks of 16 runs. Each block consisted of 16 randomly ordered runs. The first block was considered as trial, the last three blocks were the measurements. One run lasted approximately 5 min, of which the first and last 15 s were not used for analysis. After each run the pilot was asked to rate workload using the NASA Task Load indeX (TLX) subjective workload rating scale.[36] After the experiment pilots were asked to complete

an extensive questionnaire that addressed the usefulness of the augmentation forms for following the nominal trajectory.

*6. Dependent Measures*

The dependent measures were 1) path-following performance, expressed in the root-mean square (rms) of the aircraft lateral ($x_e$) and vertical ($v_e$) position errors and in the standard deviation (STD) of the aircraft lateral ($\chi_e$) and vertical ($\gamma_e$) flight-path angle errors (all measured relative to the tunnel trajectory), 2) pilot control activity, expressed by the STD of the lateral and the vertical stick deflections ($\delta_{as}$, $\delta_{es}$), the stick deflection rates ($\dot{\delta}_{as}$, $\dot{\delta}_{es}$), and the average number of control activities per time unit (decnt, dacnt), 3) ride comfort, expressed by the STD of the lateral acceleration ($\ddot{x}_e$) and vertical load factor ($N_z$), and 4) pilot workload (the TLX rating).

Note that because the concepts require different strategies in the lateral plane (e.g., the FBW concept requires a constant lateral stick deflection in turns), the stick deflections themselves were not used as measures for pilot control activity.[13,14]

### B. Description of the Experiment Simulation

*1. Tunnel-in-the-Sky Display*

In the experiment the primary interface between the pilot and the aircraft was a generic tunnel-in-the-sky display (Fig. 11). All conventional instruments were shown: speed and altitude tapes, compass rose, pitch ladder, bank and slip indicators, and vertical speed indicator. In the top part of the display the active augmentation concept was shown. The tunnel width and height were fixed at 50 m.

*2. Approach Trajectory*

The trajectory contained two turns of 80 deg, two turns of 50 deg, and four flight-path changes with a maximum descent angle of 3 deg (see Fig. 12).

*3. Aircraft Model*

The aircraft model was the nonlinear model of the Cessna Citation 500 used in the offline simulations described.

*4. Wind Model*

Above 1000 ft, wind was constant and it decreased exponentially below 1000 ft. The wind direction was only defined horizontally at a constant attitude of 30 deg with respect to the localizer, in opposite direction of the landing, mirrored for left/right approach trajectories.

### C. Experiment Hypotheses

It was hypothesized that pilot workload and control activity would be lowest and path-following performance best for the path-oriented control augmentation (FBW+). Workload and control activity were expected to be highest and performance worst for the baseline (FPV). It was hypothesized that the flight-path predictor display augmentation would rate in between the two control augmentation concepts as far as performance is concerned but also would result in higher workload and control activity.

It was hypothesized that performance would decrease and workload and control activity would increase in the heavy wind condition as compared to the normal wind for all concepts except the path-oriented augmentation.

## V. Results and Discussion

The main results of the experiment are summarized in this section.

### A. Statistical Analysis of the Dependent Measures

A full-factorial analysis of variance (ANOVA), based on a model with repeated measures, was conducted with the augmentation concept (AC, four levels) and wind condition (WC, two levels) as fixed effects and pilot as a random effect (Table 3). The means and the 95% confidence limits of the dependent measures are shown in Fig. 13.

*1. Path-Following Performance*

Path-following performance was significantly influenced by the augmentation concept ($x_e$: $F_{3,15} = 27.132$, $p \le 0.01$; $v_e$: $F_{3,15} = 29.344$, $p \le 0.01$; $\chi_e$: $F_{3,15} = 29.913$, $p \le 0.01$; $\gamma_e$: $F_{1,5} = 24.987$, $p = 0.004$). The wind condition significantly affected the horizontal position error ($x_e$: $F_{1,5} = 17.350$, $p = 0.009$) and, surprisingly, the flight-path angle error ($\gamma_e$: $F_{1,5} = 24.987$, $p = 0.004$).

Post hoc analysis [Student–Newman–Keuls (SNK), $\alpha = 0.05$] showed that the FPP and the FBW+ both resulted in the smallest rms $x_e$. The worst performance was shown in the baseline (FPV), as was hypothesized. The path-oriented concept had the smallest rms of $v_e$ and STD of $\gamma_e$. This is remarkable, because the design objective of the path-oriented control was to improve lateral tracking performance.

The heavy wind caused the FPV and FBW concepts to perform significantly worse than in the normal wind condition, whereas performance remained the same with the FPP and even improved with

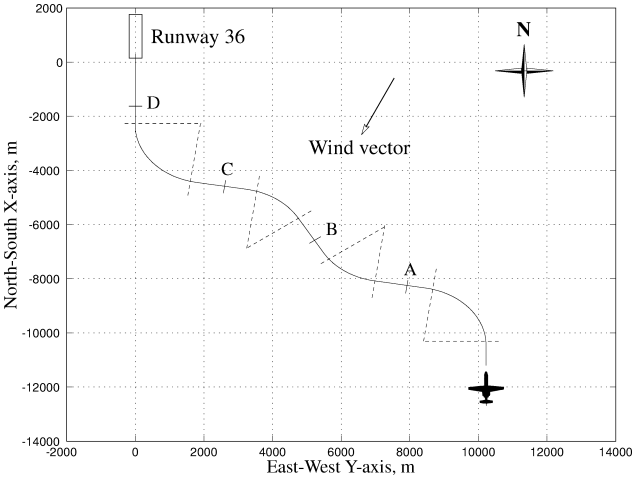


**a) Top view of the reference trajectory (left-hand orientation)**

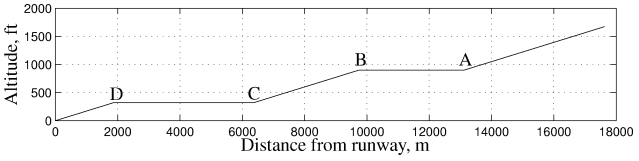


**b) Side view of the reference trajectory**

**Fig. 12 Nominal trajectory used in the experiment.**

**Table 3 Results of a full-factorial ANOVA of the dependent measures**

| | Position error | | Flight-path angle error | | Control activity | | | | Accelerations | | |
|---|---|---|---|---|---|---|---|---|---|---|---|
| Variable | $v_e$ | $x_e$ | $\gamma_e$ | $\chi_e$ | $\dot{\delta}_{es}$ | $\dot{\delta}_{as}$ | decnt | dacnt | $N_z$ | $\ddot{x}_e$ | Workload zTLX |
| Main effects | | | | | | | | | | | |
| AC | ★★ | ★★ | ★★ | ★★ | · | ★★ | · | ★★ | ★★ | ★★ | ★★ |
| WC | · | ★★ | ★★ | · | · | · | ○ | · | ○ | · | ★ |
| Two-way interactions | | | | | | | | | | | |
| AC × WC | ○ | ★★ | ★★ | ○ | · | · | · | · | · | ★★ | · |

*Note*: ★★, ★, and ○ represent chance levels of $p \le 0.01$, $0.01 < p \le 0.05$, and $0.05 < p \le 0.10$, respectively; · represents chance level of $p > 0.10$.

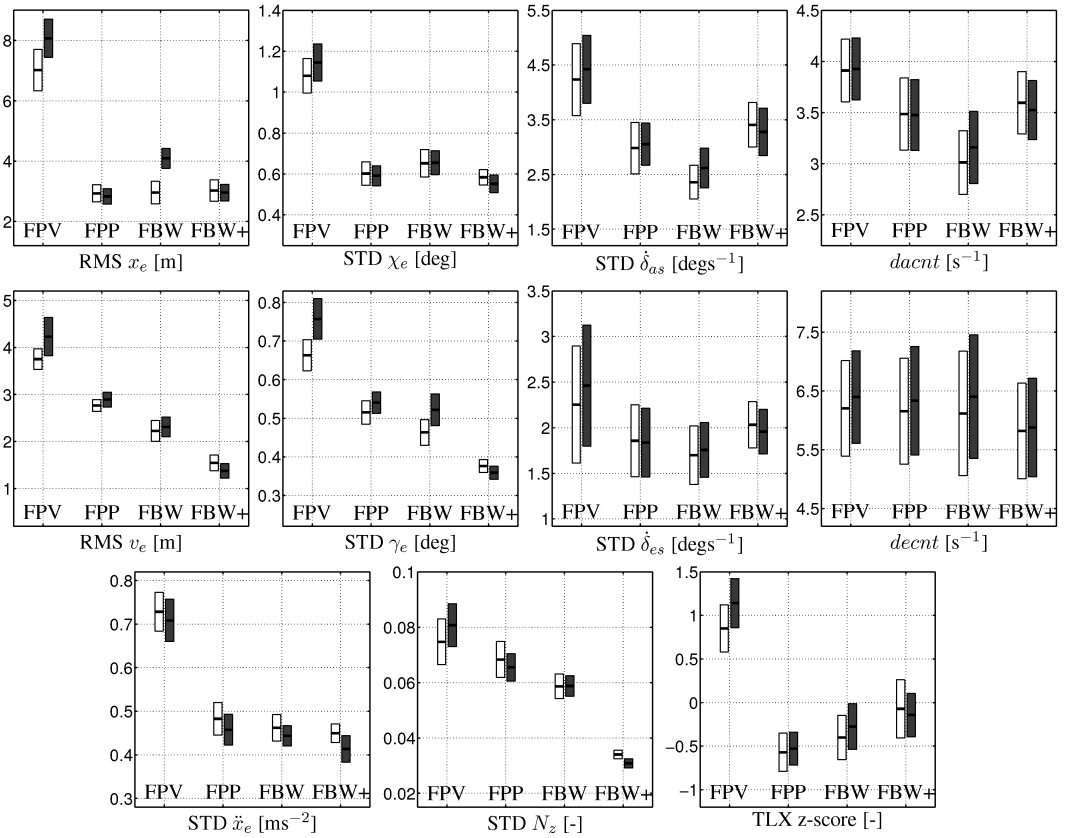


**Fig. 13 Means and 95% confidence intervals of the dependent measures (data for all subjects). The white and gray bars correspond to normal and heavy wind, respectively.**

FBW+. This resulted in the significant AC × WC interactions ($x_e$: $F_{3,15} = 19.026$, $p \leq 0.01$; $\gamma_e$: $F_{3,15} = 11.738$, $p \leq 0.01$).

*2. Control Activity*

The augmentation concept resulted in a significant effect on the lateral stick velocity and activity counter ($\dot{\delta}_{as}$: $F_{3,15} = 6.400$, $p = 0.005$; dacnt: $F_{3,15} = 15.090$, $p \leq 0.01$). These were mainly caused by the higher control activity for the baseline (FPV), as hypothesized, and the differences among the other concepts were fairly small. The wind condition had only a borderline significance on the longitudinal stick activity counter (decnt: $F_{1,5} = 5.737$, $p = 0.062$).

For the longitudinal control activity, no significant differences were found between the augmentation concepts. As was hypothesized, the FBW and baseline concepts resulted in the lowest and highest control activity, respectively. Unexpectedly, the FBW+ concept resulted in the second-highest control activity.

*3. Ride Comfort*

The vertical load factor ($N_z$) and the horizontal acceleration ($\ddot{x}_e$) were both significantly influenced by the augmentation concept ($N_z$: $F_{3,15} = 19.979$, $p \leq 0.01$; $\ddot{x}_e$: $F_{3,15} = 22.501$, $p \leq 0.01$). The highest accelerations were found for the baseline (FPV), as was hypothesized. The differences among the other concepts were negligible, except for the vertical acceleration $N_z$, which was much smaller with the FBW+ concept (SNK, $\alpha = 0.05$). In heavy wind the STD of $N_z$ increased for the baseline but decreased for the FBW+ concept, resulting in a significant AC × WC interaction ($F_{3,15} = 10.581$, $p = 0.001$).

*4. Pilot Workload Ratings*

The augmentation concept significantly affected the TLX workload rating ($F_{3,15} = 7.772$, $p = 0.002$). As hypothesized, the highest workload is reported for the baseline (FPV). The lowest workload is found for the FPP, followed closely by the FBW concept. The FBW+ concept led to the second-highest workload rating, supporting the control activity findings. The TLX ratings do not correlate perfectly with the control activity measurements, however. Pilots reported the FBW concepted result in a higher workload than the FPP, even when control activity with the former was considerably less. The heavy wind condition resulted in a significant increase in workload ($F_{1,5} = 8.974$, $p = 0.030$) for all concepts, except the FBW+, as hypothesized.

### B. Pilot Questionnaire

Pilots commented that the path-oriented augmentation concept was somewhat hard to master. Especially initiating and leaving a curve were found to be difficult. Pilots found the command tunnel to be drawn over a too-large prediction time, and because they focused mainly on matching the farthest part of the command tunnel with the reference tunnel, this contributed to "corner cutting." None of the pilots preferred the current implementation of the path-oriented augmentation, mainly because they found themselves concentrating too much on minimizing the position errors between the command and reference tunnel.

### C. Discussion of the Experimental Results

Not all experimental hypotheses were confirmed in the experiment. The path-oriented control augmentation system indeed resulted in the best path-following performance and the smoothest ride. This improved performance is accompanied by a higher control activity and pilot workload, however, which were not hypothesized. A reasonable explanation would be that the command tunnel revealed even the smallest position errors, which were invisible with the other concepts. Then, as pilots were instructed to maximize tracking performance, they could have tried to compensate for every small error, increasing their control activity and workload considerably.

The flight-path predictor display augmentation again resulted in the best balance between performance and control activity. In particular in the lateral dimension it was the best solution, with about

the same lateral performance as the path-oriented control augmentation, but with lower control activity and workload. The path-augmentation probably also involved more pilot learning because most of the evaluation pilots were experienced with the tunnel-in-the-sky display and its FPP and FBW augmentations.

The path-oriented control augmentation outperformed the other concepts in vertical position tracking. Because path-oriented augmentation was developed to improve lateral tracking, this was unexpected. Because the vertical control laws of the FBW and FBW+ concepts were identical, the improvement of FBW+ over FBW in vertical tracking performance is most probably caused by the visualization of the future vertical command trajectory by the command tunnel. A similar result was found in an earlier experiment that investigated landing a HL-20 lifting body.[37] It suggests that presenting the future vertical aircraft trajectory can improve pilot performance considerably, a finding that deserves more investigation.

The hypotheses regarding the wind condition were confirmed by the experiment. In heavy wind all configurations performed worse and led to higher control activity and workload, whereas with the path-oriented augmentation performance improved, at constant levels of control activity and workload. This result could imply that when the pilot task difficulty increases, the benefits of the new path-augmentation system become more apparent. A possible explanation for the deteriorating lateral tracking performance with FBW is that in heavy wind the aircraft is skewed relative to the tunnel. Then, the highlighted command FPV reference frame becomes a parallelogram, complicating the task of placing the command FPV symbol in its center.

Future research aims to improve the path-oriented control and display augmentation and make it more straightforward to use. Curve interception could be improved through determining the "optimal" length of the command tunnel (i.e. the FTS time $T_{\text{fts}}$), balancing between cutting corners (FTS time too large) and missing a turn (FTS time too small).

Future experiments with the path-oriented control augmentation should be conducted in more realistic environments, such as a moving base simulator, and with more complex tasks. In the present experiment pilots could allocate all their attention to the position-tracking task. Tentatively, it is hypothesized that when other tasks are introduced, performance with the control augmentation systems remains fairly constant but deteriorates with the display augmentation as these concepts still require pilots' full attention in terms of control. In control-augmentation systems the pilot is taken out of the inner control loops but remains in command of the "where-to-go" loop. The simplified control task leaves more room for focusing on other tasks besides maximizing tracking performance. Another aspect is the presence of atmospheric turbulence. Whereas the control-augmentation systems automatically compensate for these disturbances, the baseline and flight-path predictor solutions do not. Previous experiments showed that this has a significant effect on pilot workload.[14,31]

## VI. Conclusions

In its present form the path-oriented control augmentation is not a significant improvement. Although it provided the smoothest ride and superior path-following performance of all concepts, it increased pilot workload and control activity. Pilots found that the path-oriented augmentation captured their attention and made them less aware of the overall situation. For future research conducting further experiments with the described control and display augmentations in a full-flight simulator is recommended to examine the hypothesis that effects of turbulence and a more complex task environment could demonstrate the potential value of control augmentation.

## Appendix: Reference Frames and Kinematics

### Definition of Reference Frames

Figure A1 shows a top view of the reference frames (along with their relations in the lateral plane). The reference frames used for this paper are inertial ($\mathcal{F}^i$), geodetical ($\mathcal{F}^g$), body ($\mathcal{F}^b$), aerodynamic ($\mathcal{F}^a$), and kinematic ($\mathcal{F}^k$).[7,32,38]

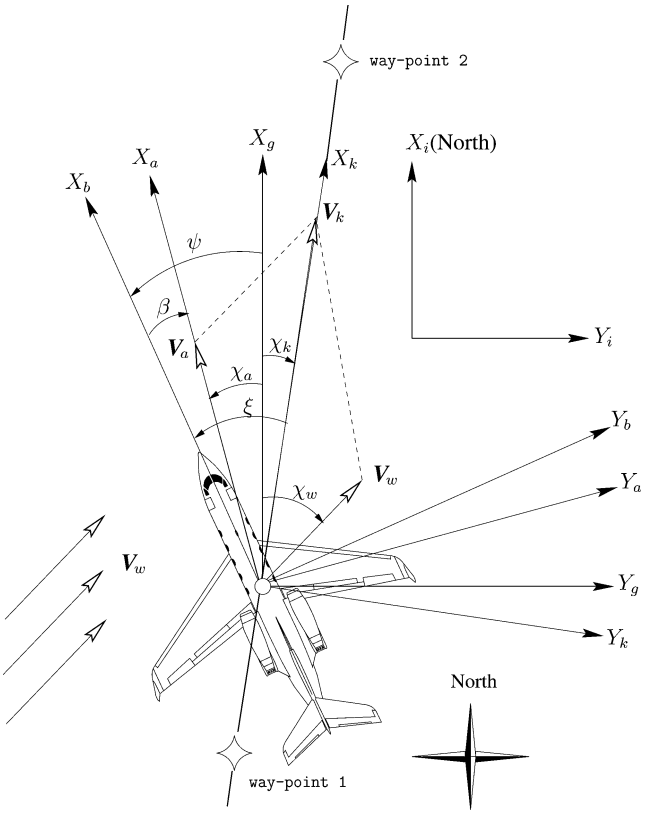


**Fig. A1 Top view of the kinematic relations and reference frames. In this figure $\chi_a$, $\xi$, and $\psi$ are negative and $\chi_k$, $\chi_w$, and $\beta$ are positive.**

### Aircraft Velocity Vectors

Figure A1 shows that the aircraft velocity relative to the ground, the kinematic velocity $\boldsymbol{V}_k$, is the vector sum of the wind velocity $\boldsymbol{V}_w$ and the aerodynamic velocity $\boldsymbol{V}_a$[32]:

$$\boldsymbol{V}_k = \boldsymbol{V}_a + \boldsymbol{V}_w \tag{A1}$$

If the aircraft is coordinated, the side slip angle $\beta$ is zero and hence the heading angle $\psi$ equals the aerodynamic azimuth angle $\chi_a$:

$$\psi = \chi_a \qquad \text{if } \beta = 0 \tag{A2}$$

This implies that now the $X_a$-axis of $\mathcal{F}^a$ lies in the symmetry plane of the aircraft. It is assumed that all aircraft are coordinated, such that $\chi_a$ can be referred to as the heading angle and $\chi_k$ as course. In a straight flight, the crab angle $\xi$ (also known as the wind correction angle) is defined as the rotation angle of an aircraft about its vertical axis so as to cause the aircraft's longitudinal axis to deviate from the flight path relative to the Earth's surface. If the aircraft is coordinated, the crab angle can be calculated from the heading angle and course angle as follows:

$$\xi = \chi_a - \chi_k \tag{A3}$$

By adopting a certain crab angle, the pilot ensures that the aircraft will be carried by the wind onto the desired Earth-fixed trajectory.

## References

[1]Grunwald, A. J., and Merhav, S. J., "Effectiveness of Basic Display Augmentation in Vehicular Control by Visual Field Cues," *IEEE Transactions on Systems, Man, and Cybernetics*, Vol. SMC-8, No. 8, September 1978, pp. 679–690.

[2]Grunwald, A. J., Robertson, J. B., and Hatfield, J. J., "Experimental Evaluation of a Perspective Tunnel Display for Three-Dimensional Helicopter Approaches," *Journal of Guidance and Control*, Vol. 4, No. 6, 1981, pp. 623–631.

[3]Grunwald, A. J., "Tunnel Display for Four-Dimensional Fixed-Wing Aircraft Approaches," *Journal of Guidance, Control, and Dynamics*, Vol. 7, No. 3, 1984, pp. 369–377.

[4]Grunwald, A. J., "Predictor Laws for Pictorial Flight Displays," *Journal of Guidance, Control, and Dynamics*, Vol. 8, No. 5, 1985, pp. 545–552.

[5]Grunwald, A. J., "Improved Tunnel Display for Curved Trajectory Following: Control Considerations," *Journal of Guidance, Control, and Dynamics*, Vol. 19, No. 2, March–April 1996, pp. 370–377.

[6]Grunwald, A. J., "Improved Tunnel Display for Curved Trajectory Following: Experimental Evaluation," *Journal of Guidance, Control, and Dynamics*, Vol. 19, No. 2, March–April 1996, pp. 378–384.

[7]Mulder, M., *Cybernetics of Tunnel-in-the-Sky Displays*, Ph.D. Dissertation, Faculty of Aerospace Engineering, Delft Univ. of Technology, Nov. 1999.

[8]Lambregts, A. A., and Cannon, D. G., "Development of a Control Wheel Steering Mode and Suitable Displays that Reduce Pilot Workload and Improve Efficiency and Safety of Operation in the Terminal Area and in Windshear," *Proceedings of the AIAA Guidance, Navigation, and Control Conference*, AIAA, New York, 1979, pp. 609–620; also AIAA Paper 79-1887.

[9]Stewart, E. C., Ragsdale, W. A., and Wunschel, A. J., "An Evaluation of Automatic Control System Concepts for General Aviation Airplanes," *Proceedings of the AIAA Atmospheric Flight Mechanics Conference*, AIAA, Washington, DC, 1988, pp. 330–343; also AIAA paper 88-4364-CP.

[10]Stewart, E. C., "A Piloted Simulation Study of Advanced Controls and Displays for Novice General Aviation Pilots," *Proceedings of the 32nd AIAA Aerospace Sciences Meeting*, AIAA, Washington, DC, 1994; also AIAA Paper 1994-0276.

[11]Mulder, M., Veldhuijzen, A. R., Van Paassen, M. M., and Bennani, S., "Fly-by-Wire Control and Tunnel-in-the-Sky Displays: Towards a Task-Oriented Control/Display System," AIAA Paper 2002-4928, 2002.

[12]DeClercq, J., Mulder, M., and Van Paassen, M. M., "Integrating Fly-by-Wire and Tunnel-in-the-Sky Displays for Large Transport Aircraft," AIAA Paper 2004-5235, 2004.

[13]Mulder, M., Veldhuijzen, A. R., Van Paassen, M. M., and Mulder, J. A., "Integrating Fly-by-Wire Controls with Perspective Flight-Path Displays," *Journal of Guidance, Control, and Dynamics*, Vol. 28, No. 6, 2005, pp. 1263–1274.

[14]Lam, T. M., Mulder, M., Van Paassen, M. M., and Mulder, J. A., "Comparison of Control and Display Augmentation for Perspective Flight-Path Displays," *Journal of Guidance, Control, and Dynamics*, Vol. 29, No. 3, 2006, pp. 564–578.

[15]Grunwald, A. J., "Predictor Laws for Pictorial Flight Displays," *Journal of Guidance, Control, and Dynamics*, Vol. 8, No. 5, Sept.–Oct. 1985, pp. 545–552.

[16]Morello, S. A., Knox, C. E., and Steinmetz, G. G., "Flight-Test Evaluation of Two Electronic Display Formats for Approach to Landing Under Instrument Conditions," NASA TP-1085, Dec. 1977.

[17]Kelley, W. W., "Simulator Evaluation of a Flight-Path Angle Control System for a Transport Airplane with Direct Lift Control," NASA TP-1116, March 1978.

[18]Hamer, H. A., and Johnson, K. G., "Effects of Errors on Decoupled Control Systems," NASA TP 1184, July 1978.

[19]Miller, G. K., Jr., "Fixed-Base Simulation Study of Decoupled Longitudinal Controls During Approach and Landing of a Medium Jet Transport in the Presence of Windshear," NASA, TP-1519, Oct. 1979.

[20]Steinmetz, G. G., "Simulation Development and Evaluation of an Improved Longitudinal Velocity Vector Control-Wheel Steering Mode and Electronic Display Format," NASA TP-1664, Aug. 1980.

[21]Miller, G. K., Jr., "Simulation Comparison of a Decoupled Longitudinal Control System and a Velocity Vector Control Wheel Steering System During Landings in Windshear," NASA TP-1734, Nov. 1980.

[22]Lam, T. M., Mulder, M., and Van Paassen, M. M., "Comparison Between Augmentation Techniques for Tunnelin-the-Sky Displays," AIAA Paper 2004-5238, 2004.

[23]Borst, C., Mulder, M., and Van Paassen, M. M., "Fly-by-Wire and Tunnel-in-the-Sky Displays: Development and Experimental Evaluation of a Path-Oriented Control Augmentation," AIAA Paper 2004-5236, 2004.

[24]Sankrithi, M. K. V., and Bryant, W. F., "7J7 Manual Flight Control Functions," *Proceedings of the AIAA Guidance, Navigation, and Control Conference*, AIAA, Washington, DC, 1987, pp. 905–913; also AIAA Paper 87-2454.

[25]Van der Geest, P., Nieuwpoort, A., and Borger, J., "A Simulator Evaluation of Various Manual Control Concepts for Fly-by-Wire Transport Aircraft," *Proceedings of the AIAA Guidance, Navigation, and Control Conference*, AIAA, Washington, DC, 1992, pp. 181–191; also AIAA Paper 1992-4328.

[26]Verspay, J. J. L. H., de Myunck, R. J., Nibbelke, R. J., Van den Bosch, J. J., Kolstein, G., and Van Gelder, C. A. H., "Simulator Evaluation on Control and Display Issues for a Future Regional Aircraft," *Proceedings of the AIAA Atmospheric Flight Mechanics Conference*, AIAA, Reston, VA, 1996, pp. 176–189; also AIAA Paper 1996-3382.

[27]Veldhuijzen, A. R., *Integrating Flight Path Oriented Control with the Tunnel-in-the-Sky Display—A Promising New Concept for the Primary Interface Between Pilot and Aircraft*, MSc. Thesis, Faculty of Aerospace Engineering, Delft Univ. of Technology, Nov. 2002.

[28]Van de Vegte, J., *Feedback Control Systems*, 3rd ed., Prentice–Hall, Englewood Cliffs, NJ, 1994.

[29]Ogata, K., *Modern Control Engineering*, international ed., Prentice–Hall, Upper Saddle River, NJ, 1997.

[30]Mulder, M., Kraeger, A. M., and Soijer, M.W., "Delft Aerospace Tunnel-in-the-Sky Flight Tests," AIAA Paper 2002-4929, 2002.

[31]Mulder, M., and Mulder, J. A., "A Cybernetic Analysis of Perspective Flight-Path Display Dimensions," *Journal of Guidance, Control, and Dynamics*, Vol. 28, No. 3, 2005, pp. 398–411.

[32]Boiffier, J.-L., *Dynamics of Flight: The Equations*, Wiley, New York, 1998.

[33]McRuer, D., Ashkenas, I., and Graham, D., *Aircraft Dynamics and Automatic Control*, Princeton Univ. Press, Princeton, NJ, 1973.

[34]Blakelock, J. H., *Automatic Control of Aircraft and Missiles*, Wiley, New York, 1965.

[35]Van der Linden, C. A. A. M., "DASMAT: The Delft University Aircraft Simulation Model and Analysis Tool," Rept. LR-781, Delft Univ. of Technology, Faculty of Aerospace Engineering, April 1996.

[36]Hart, S. G., and Staveland, L. E., *Development of NASA-TLX (Task Load Index): Results of Empirical and Theoretical Research, Human Mental Workload*, edited by P. A. Hancock and N. Meshkati, Elsevier Science, North-Holland, 1988, pp. 139–183.

[37]Den Hartog, J. G., *The Effect of Trajectory and Display Design on the Handling Qualities of a Landing Lift Body*, MSc. Thesis, Faculty of Aerospace Engineering, Delft Univ. of Technology, June 2002.

[38]Ruijgrok, G. J. J., *Elements of Airplane Performance*, Delft Univ. Press, Delft, The Netherlands, 1996.